9-(Diphenylphosphoryl)-10-(phenylethynyl)anthracene Derivatives: Synthesis and Implications for the Substituent and Solvent Effects on the Light-Emitting Properties

Nina Murayama,[b] Joel Hao Jorolan,[a] Mao Minoura,[c] Haruyuki Nakano,[d] Tadaaki Ikoma,*[a] and Yoshihiro Matano*[a]

Herein, we report a series of 9-(diphenylphosphoryl)-10-(phenylethynyl)anthracenes (DPPPEAs) as novel fluorescent 9,10-disubstituted anthracene derivatives. The DPPPEAs were prepared by Sonogashira coupling of (10-bromoanthracen-9-yl)diphenylphosphine oxide with terminal arylacetylenes, and their structures were fully characterized. UV/Vis fluorescence spectroscopy and theoretical calculations were used to evaluate substituent effects on fluorescence properties of DPPPEAs. The nature of emissive excited state of DPPPEAs was found to vary greatly depending on the substituent, solvent, and temperature. Unsubstituted DPPPEA emitted intense fluorescence from locally excited (LE) state, whereas donor-acceptor (D-A) type DPPPEAs substituted with diphenylamino groups showed strong solvatofluorochromism derived from the charge-transfer (CT) state. Notably, carbazolyl derivatives exhibited fluorescence from LE hybridized with CT state. The disappearance of CT emission in rigid media suggests that solvent reorganization plays a crucial role in producing large Stokes shifts of D-A type derivatives. The DPPPEAs have also been found to function as annihilators in porphyrin-sensitized triplet–triplet annihilation processes.

Introduction

The peripheral functionalization of anthracene at the 9,10-positions has been identified as a promising strategy with implications for the electronic structures and optical properties of the anthracene ring, and the energy levels of the highest occupied molecular orbital (HOMO) and the lowest unoccupied molecular orbital (LUMO) of the anthracene unit, along with the characteristics of its singlet excited state (S_1) and triplet excited state (T_1), can be finely tuned.[1] Several chemically stable 9,10-disubstituted anthracenes have been reported for use in materials. Among these, 9,10-bis(phenylethynyl)anthracene (BPEA; Figure 1) is a well-known emitting material owing to its intrinsically high fluorescence quantum yield (Φ_F) and separated S_1 and T_1 energies.[2] In this regard, BPEA and its derivatives have been widely used as key components in the triplet-triplet annihilation (TTA) process and singlet fission process, solar cells, and luminescent liquid crystals.[3] In connection with the rich chemical properties of BPEA, the unsymmetrically substituted 9-phenylethynylanthracene (PEA) derivatives have also been developed and their tunable electronic properties have been revealed.[4]

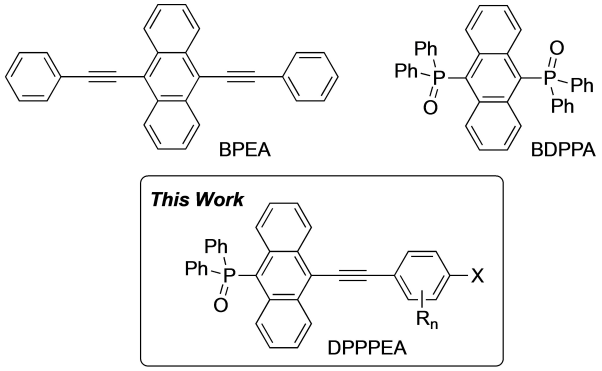

Figure 1. Structures of BPEA, BDPPA, and DPPPEA.

The diphenylphosphoryl (Ph_2PO) group possesses an electron-withdrawing property, which results in lowering the HOMO and LUMO energy levels of the adjacent π-electron system. In addition, the Ph_2PO group behaves as a Lewis-basic site for complexing metals, cations, and protons through coordination, electrostatic interaction, and/or hydrogen-bonding interaction. In the materials field, the Ph_2PO-appended aromatic hydrocarbons and heterocycles have been used as both electron-transporting blue-emitters and thermally activated delayed fluorescence dyes.[5] The luminescence and electron-transporting properties of 9,10-bis(diphenylphosphoryl)anthracene (BDPPA; Figure 1) have

[a] Prof. Dr. J. Hao Jorolan, Prof. Dr. T. Ikoma, Y. Matano
Department of Chemistry, Faculty of Science, Niigata University,
Nishi-ku, 950-2181 Niigata (Japan)
E-mail: matano@chem.sc.niigata-u.ac.jp
ikoma@chem.sc.niigata-u.ac.jp
[b] N. Murayama
Department of Fundamental Sciences, Graduate School of Science and Technology, Niigata University,
Nishi-ku, 950-2181 Niigata (Japan)
[c] Prof. Dr. M. Minoura
Department of Chemistry, College of Science, Rikkyo University,
Toshima-ku, 171-8501 Tokyo (Japan)
[d] Prof. Dr. H. Nakano
Department of Chemistry, Graduate School of Science,
Kyushu University, Nishi-ku, 819-0395 Fukuoka (Japan)

Supporting information for this article is available on the WWW under https://doi.org/10.1002/cptc.202200100

© 2022 Wiley-VCH GmbH

been explored by several research groups.[6–10] BDPPA has also been applied in the TTA-based up-conversion luminescence system with a platinum(II) porphyrin sensitizer because of the separated S_1 and T_1 energies (2.64 and 1.60 eV, respectively) and high Φ_f (0.95 in toluene).[7,9] In contrast, the structural integration of BPEA and BDPPA is unexplored. We envisioned that the Ph_2PO-appended PEAs would significantly change their excited-state characters from a locally-excited (LE) state to a charge-transfer (CT) state, depending on the substituent at the terminal phenyl group. Understanding the nature of the excited states generated by an irradiation of the donor-acceptor (D-A) type derivatives is particularly important for the development of new PEA-based fluorescent materials that cover a wide range of emission wavelengths. Here, we report a new strategy for modulating the fluorescence properties of 9,10-disubstituted anthracenes. A series of 9-diphenylphosphoryl-10-(phenylethynyl)anthracenes (DPPPEAs)[11] was designed and prepared as a backbone pertinent to the PEA-based fluorophores. The electronic and steric effects of the substituents (X and R; Figure 1) on the structural, optical, and photophysical properties of DPPPEAs have been investigated experimentally and theoretically. Preliminary results on the TTA measurements using DPPPEAs as annihilators and a platinum(II) porphyrin as a sensitizer are also reported.

Results and Discussion

Synthesis. Scheme 1 illustrates the synthesis of DPPPEAs containing the 1,4-phenylene linkage. Sonogashira coupling reactions of 9-bromo-10-(diphenylphosphoryl)anthracene **1**[12] with terminal arylacetylenes **2a–e** afforded the corresponding DPPPEAs **3a–e** quantitatively. Reductive deoxygenation of P–oxide **3c** with trichlorosilane in toluene at 90 °C gave phosphine **4**, which was subsequently converted to P–sulfide **5** and P–selenide **6** by treatment with elemental sulfur and selenium, respectively, in refluxing toluene.

To reveal the steric effect of the phenylene linkage on the optical properties of *para*-9*H*-carbazolyl derivatives, the xylylene-linked positional isomers **9** and **10** were prepared by the reaction of **1** with 9-(4-ethynyl-3,5-dimethylphenyl)-9*H*-carbazole **7** and 9-(4-ethynyl-2,6-dimethylphenyl)-9*H*-carbazole **8**, respectively (Scheme 2). The synthesis of **7** and **8** is described in the Supporting Information (SI). The DPPPEAs **3**, **5**, **6**, **9**, and **10** thus prepared were purified by silica-gel column chromatography and isolated as yellow or orange solids by recrystallization from appropriate solvents.

Structures. The structures of **3**, **5**, **6**, **9**, and **10** were fully characterized by NMR spectroscopy, IR spectroscopy, high-resolution electrospray ionization (HR-ESI) mass spectrometry, and X-ray crystallography. The ^{1}H NMR spectra of **3a–e** in $CDCl_3$ showed doublet signals at 8.05–8.67 and 8.70–8.90 ppm, which were assigned as the anthracene-ring protons at the 1,8- and 4,5-positions, respectively, based on the ^{1}H–^{1}H COSY and NOESY techniques. The Ph_2PE substituents (E = O, S, Se) caused an upfield shift of the peripheral protons at the 1,8-positions compared to those at the 4,5-positions. In addition, the $\delta_{H(1,8)}$ value of **3c** (8.62 ppm) was more deshielded than those of **5** (8.05 ppm) and **6** (8.05 ppm), reflecting the spatial electronic effect of the P=E groups on the neighboring peripheral protons.[13] The ^{31}P{^{1}H} NMR spectra of **3–6**, **9**, and **10** in $CDCl_3$ exhibited the inherent signals due to the P-functional groups. In the ^{31}P{^{1}H} NMR spectrum of **6**, the satellite peaks derived from the ^{31}P–^{77}Se coupling were observed with a $^1J_{PSe}$ value of 730 Hz, which was slightly less than that of the Ph_3P=Se ($^1J_{PSe}$ = 732.4 Hz).[14] This indicates that the electron-donating property of the phosphorus center in **4** is slightly weak compared to that in triphenylphosphine. The IR spectra of **3**, **9**, and **10** showed the P=O stretching vibration bands at 1169–1185 cm^{-1}.

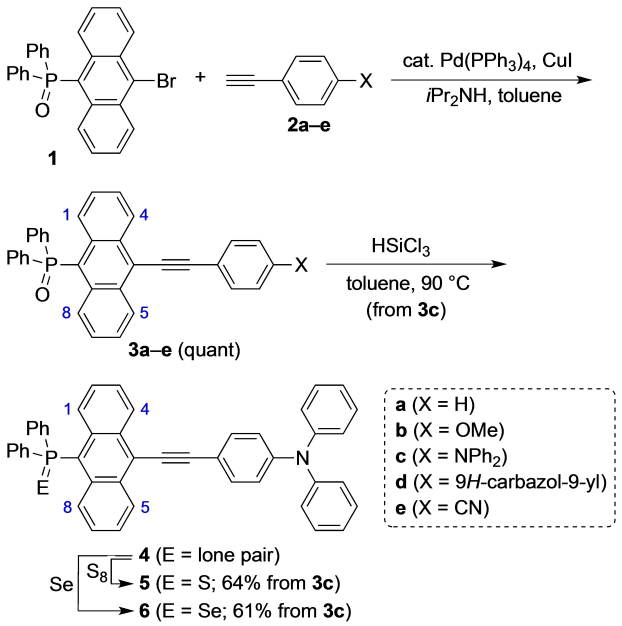

Scheme 1. Synthesis of **3**–**6**. The numbering is indicated in blue.

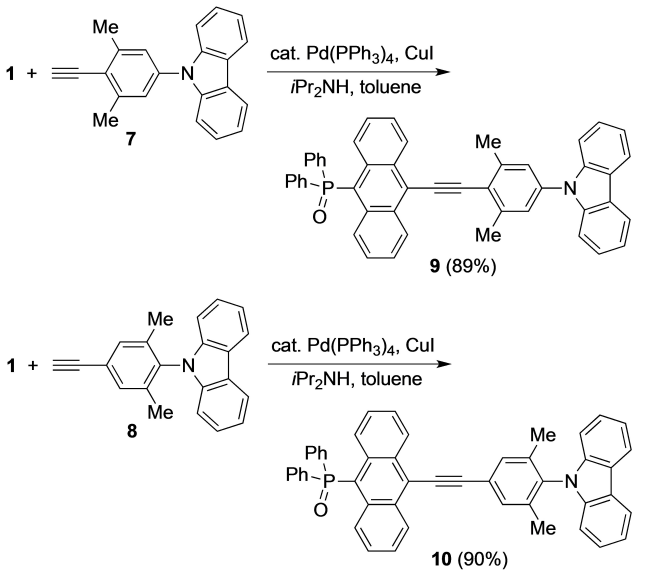

Scheme 2. Synthesis of **9** and **10**.

© 2022 Wiley-VCH GmbH

The structures of **3a**, **3c**, **3e**, **9**, and **10** were unambiguously elucidated by the single-crystal X-ray diffraction analysis. The ORTEP diagrams and selected bond parameters are shown in Figures 2 (for **3a**, **3c**, **9**, **10**) and S1 (for **3e**). The other structural parameters are summarized in Table S2. In these compounds, the phosphorus center adopts an intrinsically tetrahedral geometry with the C–P–O and C–P–C bond angles of 108–116° and 101–112°, respectively. The P=O bond lengths [1.487(1)–1.493(1) Å] and the C≡C bond lengths [1.197(3)–1.204(3) Å] are almost identical for all the derivatives and very close to the corresponding values reported for BDPPA (P=O; 1.49 Å)[6] and BPEA (C≡C; 1.20 Å).[15] The orientation of the P=O group relative to the adjacent anthracene ring varies significantly depending on the combination of the substituents. The P=O group in **3a**, **3e**, and **9** lies almost in the same plane of the anthracene ring, whereas it is mostly perpendicular in **3c** and **10**. The relative orientation of the P=O group is also concerned with the planarity of the anthracene ring, which is nearly flat in **3a**, **3e**, and **9** but slightly bent in **3c** and **10**. It should be noted here that the ^{1}H-NMR spectra of these compounds showed symmetrical spectral patterns with the similar chemical shifts for the peripheral 1,8-protons of the anthracene ring (vide supra). This indicates that the Ph_2PO group can rotate around the P–C bond in solution. Therefore, the orientation of the Ph_2PO moiety in the crystals may be induced by the packing effect.[16]

The other structural features of the crystalline state are briefly summarized for each compound. In **3a** (Figure 2a), the anthracene and benzene rings were nearly in the same plane, indicating that their π orbitals were efficiently conjugated via an acetylene linkage. In **3c** (Figure 2b) and **3e** (Figure S1), the phenylene spacer was twisted from the anthracene mean π-plane with a dihedral angle of 51.8° and 24.8°, respectively. The three *N*-bound benzene rings in **3c** had propeller-like conformations. In **9** (Figure 2c), the xylene ring was twisted from the anthracene and carbazole mean π-planes with a dihedral angle of 39.2° and 53.6°, respectively, and the carbazole ring was perpendicular to the anthracene ring. The co-crystallized methanol molecule coordinated to the Ph_2PO group through the hydrogen-bonding interaction. In **10** (Figure 2d), the xylene ring was considerably twisted from the anthracene and carbazole mean π-planes with a dihedral angle of 69.5° and 70.3°, respectively. The carbazole and anthracene rings in **10** were oriented almost parallelly, but the highly twisted xylene linker prevented an effective π-conjugation. The relative orientation of the phenylene linkers and *para*-substituents in DPPPEAs may affect the excited-state dynamics in solution (vide infra).

Optical, Electrochemical, and Photophysical Properties. The ultraviolet/visible (UV/Vis) absorption and fluorescence spectra of **3**, **5**, **9**, and **10** in CH_2Cl_2 are shown in Figure 3, and those in several solvents are summarized in Figures 4 and S2. The absorption maxima (λ_{abs}), emission maxima (λ_{em}), and fluorescence quantum yields (Φ_f) of **3**, **5**, **9**, and **10** in three solvents (toluene, CH_2Cl_2, and MeCN) are listed in Table 1. The other optical data are summarized in Table S3. The results obtained are discussed in terms of the electronic and steric effects of the substituents and the polarity of the solvents.

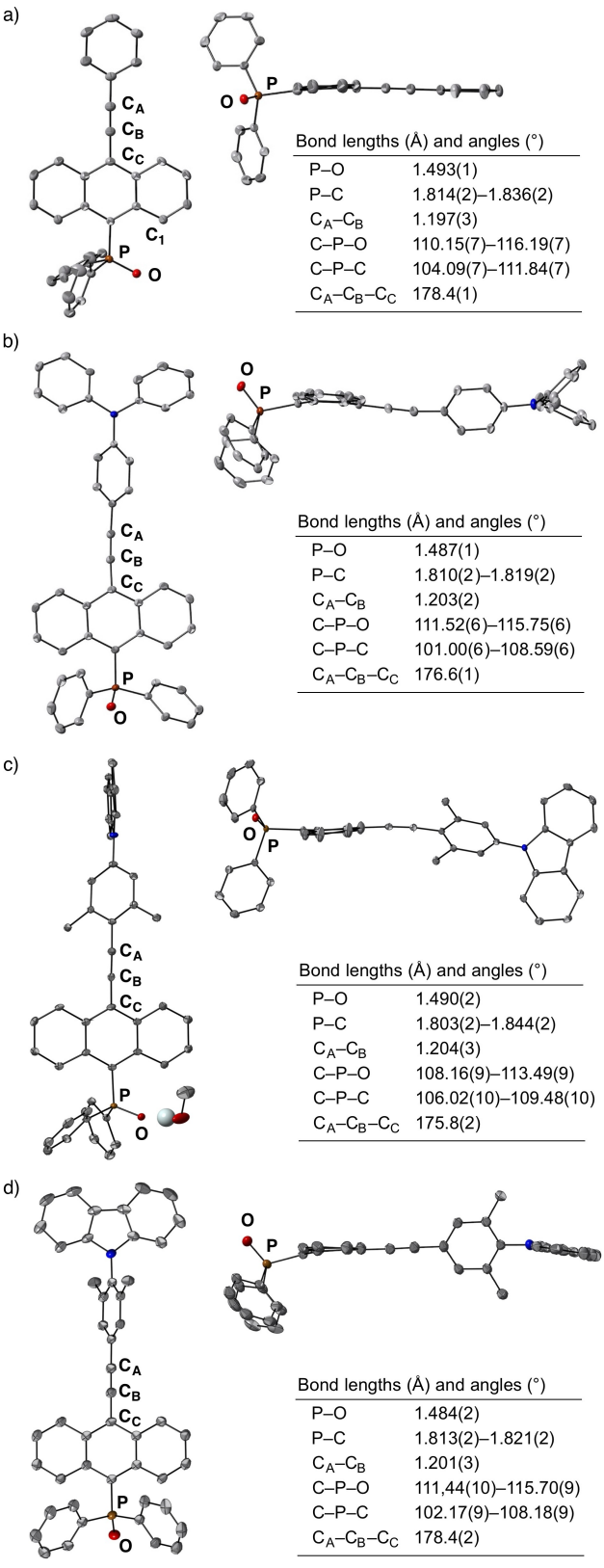

Figure 2. Top and side views (50% probability ellipsoids) and selected bond lengths and angles of a) **3a**, b) **3c**, c) **9**·MeOH, and d) **10**. Hydrogen atoms and solvents are omitted for clarity except for the MeOH in c).

© 2022 Wiley-VCH GmbH

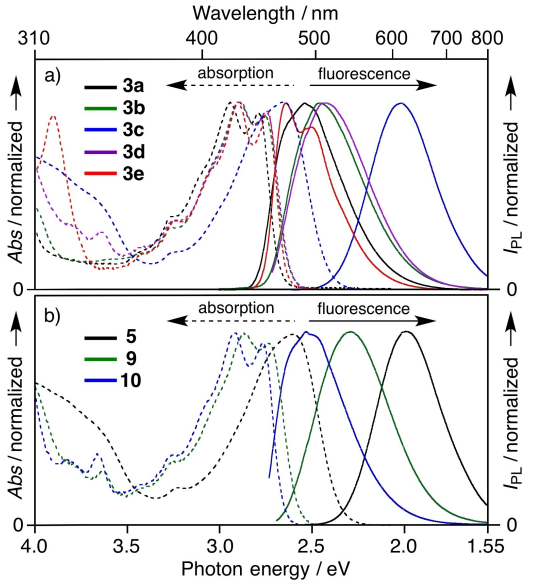

Figure 3. The normalized UV/Vis absorption and fluorescence spectra of a) **3a–e** and b) **5**, **9**, **10** in CH_2Cl_2.

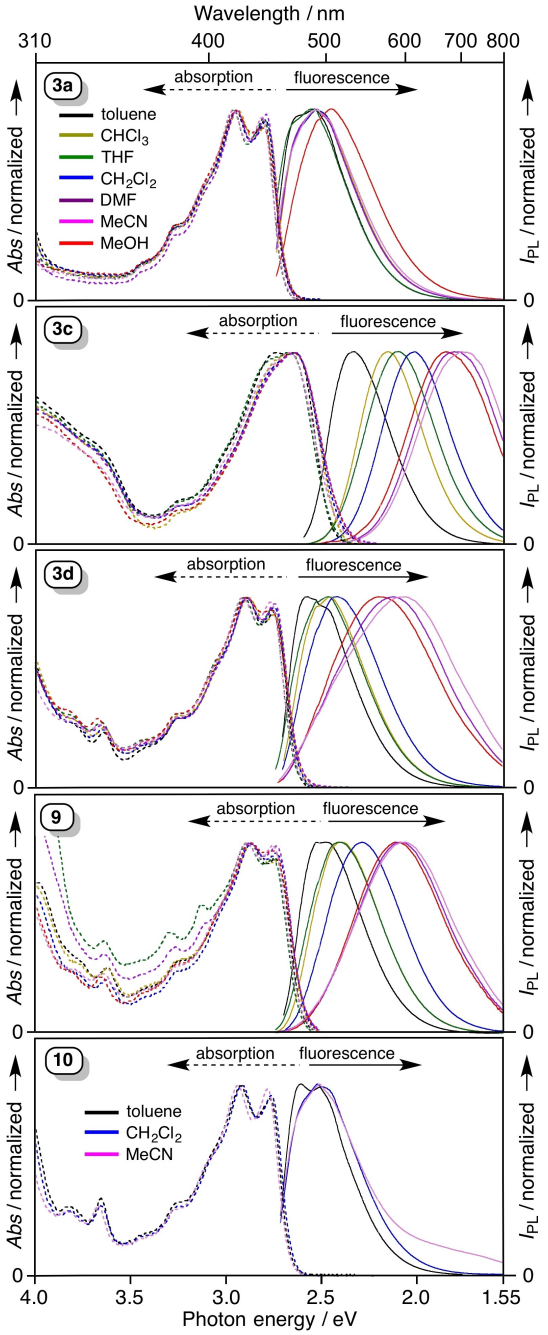

Figure 4. The normalized UV/Vis absorption and fluorescence spectra of **3a**, **3c**, **3d**, **9**, and **10** in several solvents.

Both the absorption and fluorescence spectra of **3a** and **3e** were hardly influenced by solvent polarity. The exceptional red-shift of λ_{em} in MeOH may reflect the hydrogen-bonding interaction between the P=O group and the solvent.[17] These spectral features suggest that the S_1 states of **3a** and **3e** exhibit the LE character. As shown in Figure 3a, introducing electron-donating *para*-substituents (OMe, NPh_2, 9*H*-carbazolyl) caused bathochromic shifts in the fluorescence spectra; λ_{em} increased in the order **3a** < **3b** < **3d** < **3c**. In sharp contrast to **3a**, the *para*-NPh_2 derivative **3c** showed a clear solvent dependence of λ_{em}; Stokes shifts ($\Delta\nu = \nu_{abs} - \nu_{em}$) increased in the order toluene (2530 cm^{-1}) < CH_2Cl_2 (5170 cm^{-1}) < MeCN (7330 cm^{-1}). The spectral features and solvatochromic behavior of **5** and **9** were similar to those of **3c** and **3d**, respectively. The large solvatofluorochromism observed for **3c**, **3d**, **5**, and **9** suggests that their excited states have the intrinsic CT character derived from the D-A structures consisting of amine (D) and Ph_2PO-appended PEA (A) units.

To get more insight into the electronic effects of *para* substituents, we measured the redox potentials of **3a**, **3c**, and **3d** in CH_2Cl_2 by cyclic voltammetry (CV) and differential pulse voltammetry (DPV) with Bu_4NPF_6 as a supporting electrolyte. As shown in Figures S3a–c, all voltammograms showed reversible reduction and irreversible oxidation processes. The reduction potentials (E_{red}) were within a narrow range of −1.78 to −1.84 V vs. the ferrocene/ferrocenium couple (Fc/Fc^+), which were shifted to the positive side compared to that of 9-phenyl-10-(phenylethynyl)anthracene ($E_{red} = -2.10$ V).[18] These data indicate that the LUMO level of the PEA framework is stabilized by attaching the Ph_2PO group but hardly affected by the *para* substituents. In contrast, the oxidation potentials (E_{ox}) varied widely depending on the *para* substituents; +0.94 V for **3a**, +0.54 V for **3c**, and +0.85 V for **3d**. The oxidation processes observed for **3c** and **3d** were attributed to the amine-centered oxidations by comparing with the E_{ox} of triphenylamine ($E_{ox} = +0.60$ V vs. Fc/Fc^+ under our measurement conditions) and 9-phenylcarbazole ($E_{ox} = +0.84$ V vs. Fc/Fc^+).[19] The electrochemical HOMO–LUMO gaps of **3a** (2.74 eV), **3c** (2.38 eV), and **3d** (2.63 eV) were almost identical to their optical HOMO-LUMO gaps (2.72 eV for **3a**, 2.38 eV for **3c**, 2.66 eV for **3d**) determined from the UV/Vis absorption and fluorescence spectra in CH_2Cl_2.

The molecular orbital characteristics and energies of several DPPPEAs were evaluated using the density functional theory (DFT) calculations (Figures 5 and S4). For **3a**, the HOMO and LUMO were spread over the entire PEA chromophore. For **3c**,

© 2022 Wiley-VCH GmbH

Table 1. Selected optical data for **3a–e**, **5**, **9**, and **10**.[a]

	in toluene			in CH_2Cl_2			in MeCN		
	$\lambda_{abs}/\lambda_{em}$ [nm]	Stokes shift [cm^{-1}]	Φ_f	$\lambda_{abs}/\lambda_{em}$ [nm]	Stokes shift [cm^{-1}]	Φ_f	$\lambda_{abs}/\lambda_{em}$ [nm]	Stokes shift [cm^{-1}]	Φ_f
3a	445/487	1960	0.80	445/489	2050	0.89	443/489	2130	0.80
3b	451/498	2090	n.m.	451/506	2440	0.82	447/513	2880	n.m.
3c	469/532	2530	0.82	467/616	5170	0.88	463/702	7330	0.11
3d	452/501	2160	0.94	452/511	2550	0.99	449/602	5660	0.25
3e	453/469	780	0.92	453/470	800	0.96	448/470	1000	0.78
5	478/540	2400	0.76	477/623	4910	0.87	472/721	7320	0.12
9	454/499	2010	0.91	454/540	3510	0.98	451/600	5510	0.45
10	448/489	1870	0.96	449/489	1820	0.97	446/489	1970	0.08

[a] λ_{abs} = The longest absorption maxima. λ_{em} = The shortest emission maxima. Stokes shift = $1/\lambda_{abs} - 1/\lambda_{em}$. Φ_f = The absolute fluorescence quantum yield. The other data are summarized in Table S3 in the Supporting Information. n.m. = Not measured.

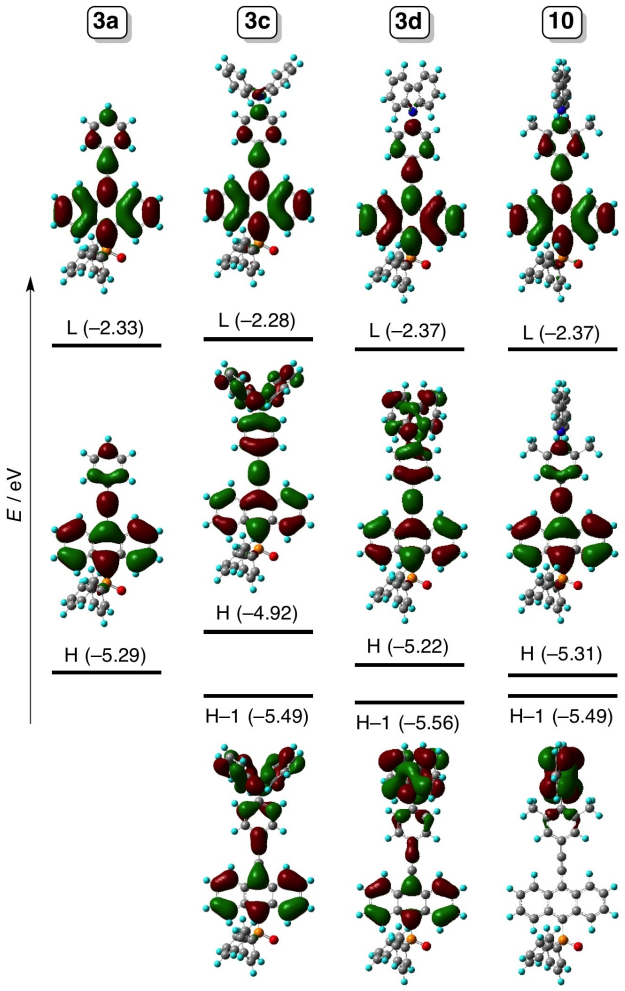

Figure 5. Selected Kohn-Sham orbitals and their energies (in eV) of **3a**, **3c**, **3d**, and **10** calculated by the DFT method (B3LYP/6-31G(d,p)) with the solvent effect (SMD, CH_2Cl_2). H = HOMO; L = LUMO.

the HOMO and HOMO–1 had characteristics derived from both the PEA-based and amine-based orbitals with an energy separation of 0.57 eV. The HOMO level of **3c** was 0.37 eV higher than that of **3a**, reflecting the electron-donating property of the *para*-NPh_2 group. The HOMO and HOMO–1 levels of **3d** were appreciably lower than those of **3c** because of the reduced electron-donating nature of its amine unit. The relative energies of the HOMOs and LUMOs of **3a**, **3c**, and **3d** calculated using the DFT method were in good agreement with those of the experimentally determined redox potentials.

Figure 6 shows the fluorescence spectra of **3c** detected in the rigid glassy solvents of methylcyclohexane (MCH) and butyronitrile (BuCN) at 77 K. The spectral shape of the fluorescence in the rigid MCH was similar to that observed in the fluid MCH at 298 K. The slight shift of the fluorescence spectrum to the low energy side may be due to an increase in the dielectric constant (ε_r) of MCH at low temperatures.[20–23] The fluorescence spectrum of **3c** in the rigid BuCN at 77 K became narrow and showed a drastic peak shift to the high energy side in comparison to that in the fluid BuCN at 298 K. The fluorescence spectra of **3d**, **5**, and **9** exhibited a similar dependence on the solvent rigidity, whereas those of **3a** did not depend on it in both the polar and nonpolar solvents (Figure S5). These results indicate that the large Stokes shifts observed for **3c**, **3d**, **5**, and **9** in polar fluid solvents are mainly due to the reorganization of solvent molecules to stabilize the CT state. The orientational motion of the solvent molecules causing the observed dynamic Stokes shift at 298 K is much slower than the optical transition from the S_0 state to the S_1 state, but it is faster than the fluorescence decay.

To discuss the solvent reorganization more quantitatively, we simulated the absorption and fluorescence spectra at 298 K as shown in Figures 6 and S5, using the spectral shape functions derived from the Franck-Condon principle.[24,25] The estimated reorganization energies for **3c**, **3d**, **5**, and **9** in BuCN (λ), which cause a broadening of the vibronic progression, are 0.57, 0.20, 0.64, and 0.46 eV, respectively. These λ are primarily due to the reorganization of BuCN molecules because the internal reorganization energies (λ_{in}) calculated for **3c** (0.121 eV) and **3d** (0.141 eV) in the gas phase are appreciably smaller than these values (for details, see page SI-7 in SI). The differences of the potential minima between the S_1 and S_0 states (ΔG) for **3c**, **3d**, **5**, and **9** in BuCN, which determine the peak position of the fluorescence ($\Delta G - \lambda$), were estimated to be 2.48, 2.74, 2.52, and 2.79 eV, respectively. Therefore, it is clarified that the substitution with the NPh_2 group (**3c**, **5**) stabilizes the energy of the CT state to a greater extent and results in having a larger reorganization energy than that with the carbazolyl group (**3d**, **9**).

© 2022 Wiley-VCH GmbH

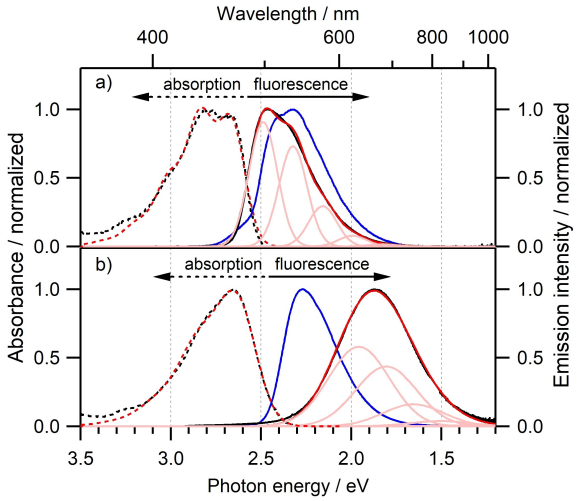

Figure 6. Fluorescence (solid line) and absorption (broken line) spectra for **3c** observed in a) MCH and b) BuCN. The black and blue curves are spectra observed at 298 K and 77 K, respectively. The red curves are simulated spectra of the absorption and fluorescence in fluid solvents at 298 K. The pink curves are vibronic lines constituting the simulated fluorescence spectra.

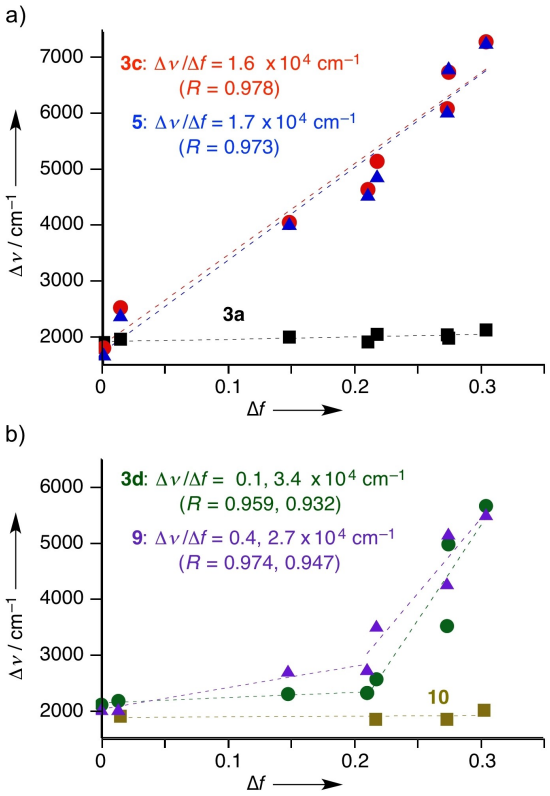

Figure 7. Lippert–Mataga plots for a) **3a** (black square), **3c** (red circle), and **5** (blue triangle) and b) **3d** (green circle), **9** (purple triangle), and **10** (yellow square). Calculated from the data for seven solvents listed in Table S3. $\Delta\nu = \nu_{abs} - \nu_{em}$; $\Delta f = (\varepsilon-1)/(2\varepsilon+1) - (n^2-1)/(2n^2+1)$. ε = dielectric constant; n = refractive index. For **3d** and **9**, the plots are analyzed using two LSERs.

As shown in Figure S3, the position of the two *ortho*-methyl groups in the positional isomers **9** and **10** was less impactful on the E_{red} (−1.78 V for **9**, −1.79 V for **10**) and E_{ox} (+0.83 V for **9**, +0.88 V for **10**). However, the fluorescence properties of compounds **9** and **10** are quite different. The fluorescence spectra of **10** in CH_2Cl_2 and MeCN were considerably blue-shifted compared to those of **9**, suggesting that **10** would have a substantial LE character in the excited state. Although the DFT-optimized structure of **10** differs from its crystal structure, there is a similarity in the distortion of the two rings around the C–N bridge. Most importantly, the carbazole ring in **10** was perpendicularly twisted against the adjacent xylene ring owing to steric constraints caused by the *ortho*-methyl groups. This distortion disturbs the efficient mixing of the PEA-based and carbazole-based orbitals; for **10**, the HOMO is located on the PEA unit, whereas the HOMO–1 is localized on the carbazole ring (Figure 5). The structural features of **10** were also reflected in the value of Φ_f, which decreased from 0.97 in CH_2Cl_2 to 0.08 in MeCN. These results may indicate that the steric constraints on the conformational change at the xylylene–carbazole linkage prevented an internal reorganization to stabilize the CT state (vide infra).

To quantitatively compare the CT properties of the excited states, we analyzed their solvatochromic shifts according to the Lippert-Mataga (L-M) theory and revealed three types of solvent dependences (type-I, -II, and -III). As shown in the L-M plot in Figure 7a, the Stokes shifts for **3a** exhibited a linear solvation energy relationship (LSER) with a negligible slope ($\Delta\nu/\Delta f$) versus the orientation polarizability (Δf) of the solvent (type-I). The absence of a solvent polarity dependence on the Stokes shifts of **3a** indicates that the electronic structure of the S_1 state is the LE state. On the other hand, the Stokes shifts of the *para*-NPh_2 derivatives **3c** and **5** showed similar LSERs (type-III), where $\Delta\nu/\Delta f$ were determined to be 1.6×10^4 and 1.7×10^4 cm^{-1}, respectively. These values suggest that the dipole moment in the S_1 state increased by 13–14 D from that in the S_0 state, which was calculated by substituting the experimental values of $\Delta\nu/\Delta f$ into the L-M equation.[26] From the large increase in the dipole moment in the S_1 state, we can assign the S_1 states of **3c** and **5** to the CT state. As shown in the L-M plots in Figure 7b, the *para*-(1-carbazolyl) derivatives **3d** and **9** exhibited a bent dependence (type-II), whereas **10** exhibited no change. Two different LSERs are depicted in the plots of **3d** and **9**. The $\Delta\nu/\Delta f$ ranges between $0.1–0.4\times10^4$ cm^{-1} for solvents with $\Delta f \leq 0.22$. However, it changes to $2.7–3.4\times10^4$ cm^{-1} for solvents with $\Delta f \geq 0.22$. These slopes correspond to the increases in the dipole moment in the S_1 state: 3–7 D in the nonpolar solvents and 17–20 D in the polar solvents. The dipole moment change in the polar solvents indicates that the S_1 state is switched between the LE and CT states depending on the polarity of the solvent. Because **10** maintains a small $\Delta\nu/\Delta f$, the fluorescence for **10** is likely to arise mostly from the LE state even in polar media. It can be concluded that the emission properties of **10** in the polar solvents, differing from **3d** and **9**, are related to the large dihedral angle between the xylylene linker and the carbazole ring.

To understand the substituent effect on the fluorescence properties of **3a**, **3c**, **3d**, and **10** in more detail, we calculated their excited state structures by the DFT method. For each

© 2022 Wiley-VCH GmbH

compound, the vertical transition energies at the optimized structures of both the S_0 and S_1 states were calculated by the time-dependent DFT (TD-DFT) method. The results are shown in Figures 8 and S4 and Table S5. The TD-DFT calculations revealed that the S_0-to-S_1 and S_1-to-S_0 transitions were essentially attributable to the electronic transitions between the HOMO and LUMO. The substituent effect on the transition energies qualitatively reflects the order of the observed λ_{abs} and λ_{em}, and the large oscillator strengths ($f = 0.581–1.214$) of the S_1-to-S_0 transitions support the highly fluorescent nature of the DPPPEAs ($\Phi_f = 0.88–0.99$) in CH_2Cl_2. The calculated dipole moments confirm that **3a**, **3c**, and **3d** in the S_1 state have the characteristics of the LE, CT, and LE hybridized with CT (denoted hereafter as LC[27]) state, respectively. Notably, the dipole moment of the S_1 state of **10** (5.4 D) is significantly smaller than that of **3d** (10.4 D), confirming that the S_1 state of **10** has essentially the LE character. The rather twisted geometry of **10** is maintained in the S_1 state, which diminishes the spatial overlap of the wavefunctions and results in an incomplete hybridization of the LE and CT states in polar solvents.

The noticeable differences between **3c** and **3d** are discussed in terms of the internal reorganization. The S_0-to-S_1 excitation resulted in a larger contribution from the cumulene-quinoid type canonical structure, as shown in Figure 8b. The degree of change in the bond lengths (ΔL) was relatively large for the acetylene unit, with the triple bond being elongated and the adjacent single bonds being shortened. The ΔL of **3d** was larger than that of **3c**, and the calculated λ_{in} of **3d** (0.141 eV) was larger than that of **3c** (0.121 eV). These data suggest that **3c** is prone to internal reorganization in the excited state than **3d**.

To gain deeper insights into the photophysical properties of DPPPEAs, we measured the Φ_f and fluorescence lifetimes (τ_f) of **3a**, **3c**, **3d**, and **5** in several solvents. All fluorescence decay profiles obeyed the first-order kinetics. The observed data are summarized in Figure 9 and Table S4, together with the radiative and non-radiative decay rate constants (k_r and k_{nr}, respectively) obtained from the Φ_f and τ_f. The Φ_f and τ_f of **3a** are largely independent of the solvent polarity, so the solvent effect on the k_r and k_{nr} is small, which is a characteristic of the emissive LE state (type-I). The Φ_f of the *para*-NPh_2 derivatives **3c** and **5** in polar solvents are smaller than those of the same derivatives in less polar ones. For **3c**, changing the solvent from CH_2Cl_2 to MeCN slightly decreased the k_r but significantly increased the k_{nr}. The photophysical data for **3c** and **5** suggest that solvent reorganization takes place rapidly to stabilize the CT state, which reduces the Φ_f mainly due to the energy gap law for the non-radiative transition. It is notable that the k_r of the *para*-carbazolyl derivative **3d** drops down in nitriles, suggesting a switching of electronic structure. The step change between the k_r values in less polar and highly polar solvents is consistent with the observed two different LSERs in the L–M plot for **3d** (type-II).

Figure 10 illustrates the possible potentials of the S_0 and the low-lying excited singlet states for the DPPPEAs, which are

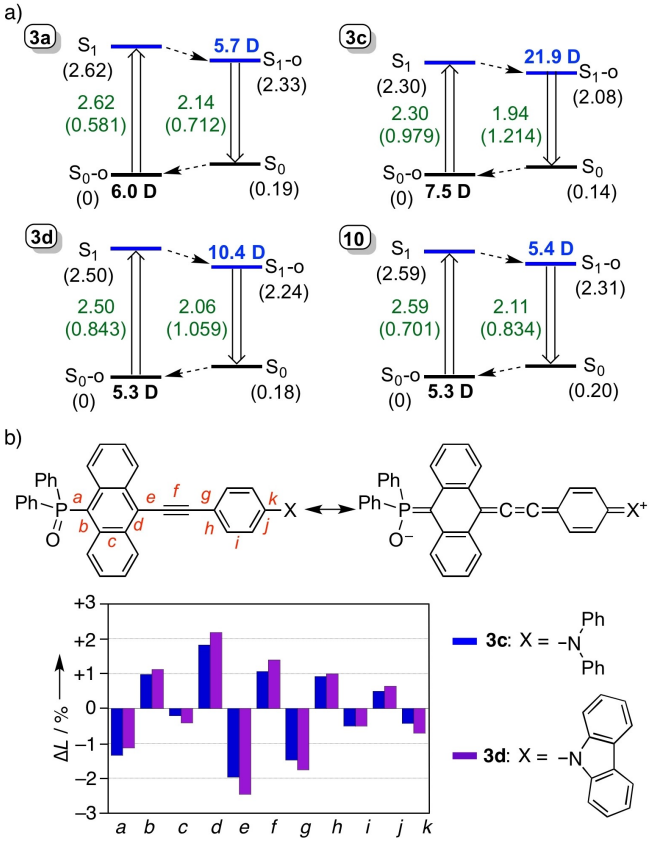

Figure 8. a) Energy diagrams of the ground and excited states calculated by the DFT method. The relative energies (in eV) are indicated in black in parentheses. S_0-o and S_1-o denote the optimized S_0 and S_1 structures, respectively. Dipole moments at the S_0-o and S_1-o states are indicated in bold. Transition energies (in eV) and oscillator strengths (in parentheses) calculated by the TD-DFT method are indicated in green. The S_0-to-S_1 excitation decreases the negative Mulliken charge of the N atom ($\Delta = +0.007$ for **3c**, $+0.010$ for **3d**) but increases that of the O atom ($\Delta = -0.004$ for **3c**, -0.010 for **3d**), resulting in an increase in the dipole moment in the S_1 structure. b) Degrees of change in the bond lengths of the S_0 state (L_{S0}) and S_1 state (L_{S1}) calculated for **3c** and **3d**. $\Delta L = (L_{S1} - L_{S0})/L_{S0} \times 100$ [%].

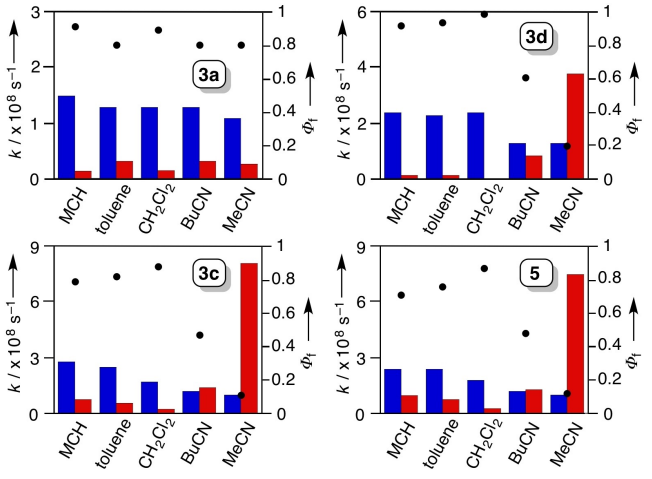

Figure 9. Fluorescence quantum yields (Φ_f; black circle plot) and radiative (k_r; blue bar graph) and nonradiative (k_{nr}; red bar graph) rate constants of **3a**, **3c**, **3d**, and **5** in solution.

© 2022 Wiley-VCH GmbH

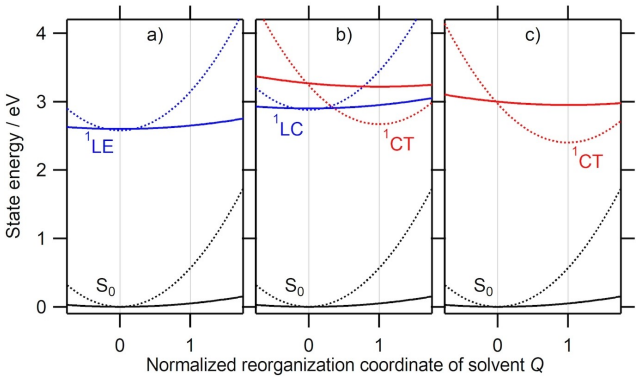

Figure 10. Plausible potentials of the S_0 state and the low-lying excited singlet states for type-I a), -II b) and -III c) in nonpolar (solid line) and polar (dot line) fluid solvents.

proposed based on the experimental results on the substituent and solvent effects on the absorption and emission spectra, the spectral simulations, and the results calculated by the DFT method. The parabolic potentials do not greatly vary with the change of reorganization coordinate of a nonpolar solvent, whereas they change drastically in a polar solvent. Since the dipole moment in the ^{1}LE state is similar to that in the S_0 state, a position in the reorganization coordinate where the energy of the ^{1}LE potential becomes minimum is the same as that of the S_0 state. The minimum position in the potential of the ^{1}CT state with a large dipole moment is known to be different from that in the S_0 state potential. We approximately set the minimum position of the ^{1}LC potential to be the same as that of the S_0 state because the dipole moment of the ^{1}LC state is closer to that of the S_0 state than to the ^{1}CT state.

According to the L-M plots, the DPPPEA derivatives are divided into three groups type-I (**3a** and **3b**), -II (**3d** and **9**) and -III (**3c** and **5**). Figures 10a, b, and c represent type-I, -II, and -III, respectively. The observed state switching between the ^{1}LC and ^{1}CT by the replacement of solvent can be understood based on an assumption that the type-II possesses the ^{1}CT state close to the ^{1}LC state which is different from the type-I and -III. The reorganization energy determining the potential curvature increases with increasing the solvent polarity. In nonpolar solvent the energy of the ^{1}LC state is lower than that of the ^{1}CT state, but the energy of the ^{1}CT state in solvents with high polarities over a certain value is lower than that of the ^{1}LC state. Therefore, in a polar solvent, the ^{1}LC state generated by photo-absorption can transfer to the ^{1}CT state at the potential intersection by solvent reorganization. For this internal conversion of ^{1}LC-to-^{1}CT, the electronic interaction of electron transfer is an important factor because the electronic structure is substantially different between the ^{1}LC and ^{1}CT states. Compounds **3d** and **9** exhibit the ^{1}LC-to-^{1}CT conversion. However, the conversion cannot occur for **10** possibly due to the small electronic coupling caused by the twisting structure of its carbazole group. The dynamic Stokes shift observed for the type-III is interpreted in terms of the potentials of Figure 10c.

Triplet-triplet annihilation. The T_1 energy for **3a** (1.45 eV) calculated by the DFT method, the sum of which is larger than the 0–0 band of fluorescence (ca. 2.6–2.7 eV), suggested that the DPPPEA would behave, similar to BPEA and BDPPA, as an emitter in the TTA. To verify this prediction, we measured the emission of **3a** and **9** (1×10^{-3} M) in several solvents at room temperature, in which platinum(II) complex of 2,3,7,8,12,13,17,18-octaethylporphyrin (PtOEP, 1×10^{-5} M) with a T_1 energy of 1.9 eV[28] was also dissolved as a triplet sensitizer. Upon irradiation of the sample solutions with a nanosecond pulse laser, using a wavelength of 532 nm (2.33 eV) to excite the Q band of PtOEP, the emission spectra shown in Figure S6 were observed in a range of less than 2.5 eV. The shapes of these emission spectra were similar to those of the fluorescence spectra obtained by the direct excitation of the DPPPEA, although the absorption and phosphorescence of PtOEP influenced the spectral shapes, resulting in slight distortions.

The time profiles of the fluorescence intensity observed by the excitation of PtOEP are different from those of the direct excitation as depicted in Figure 11. The fluorescence rose in the time range of 10^{-7} s after a prompt emission decayed in 10^{-9} s and gradually decreased in the range of 10^{-6}–10^{-5} s. The photon number for the prompt fluorescence (PF) decayed in 10^{-9} s, and was less than that of the delayed fluorescence (DF), which appeared later than 10^{-7} s. The major DF exhibited the TTA of DPPPEA producing the S_1 state,[29] although the minor PF indicated the unintentional direct excitation of concentrated DPPPEA in the solutions and/or the sensitization of DPPPEA by the S_1 state of PtOEP, which can be avoided by a proper choice of the sensitizer. This triplet sensitization experiment elucidates that the DPPPEA is a good blue-green emitter of the TTA and has the T_1 state of 1.3–1.9 eV. The solvent dependence of the DF of DPEEA was also observed.

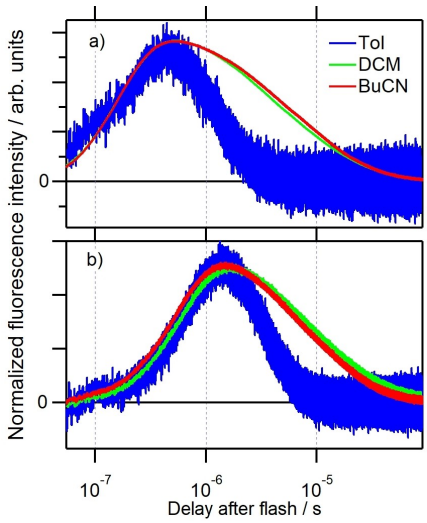

Figure 11. Time dependence of the fluorescence intensity for a) **3a** and b) **9** observed in later times after irradiating respectively **3a**/PtOEP and **9**/PtOEP in various solutions at room temperature using the nanosecond pulse with the wavelength of 532 nm.

© 2022 Wiley-VCH GmbH

Compared with the DF in CH_2Cl_2 ($\varepsilon_r = 8.9$, $\eta = 0.41$ mP·s) and BuCN ($\varepsilon_r = 24.8$, $\eta = 0.62$ mP·s), where ε_r is the relative dielectric constant and η is the viscosity coefficient, the intensity and decay in toluene ($\varepsilon_r = 2.4$, $\eta = 0.59$ mP·s) were weak and fast, respectively, even though their rise was almost similar. The TTA is sensitive to the polarity rather than the viscosity of the solvent. This suggests that the TTA efficiency reduces due to the fast natural T_1-to-S_0 decay for the DPPPEA in nonpolar solvent.

Conclusion

We synthesized the first examples of DPPPEAs by sequential Sonogashira coupling reactions and fully elucidated their structures using spectroscopic methods and X-ray crystallography. The pronounced electronic effect of the *para*-substituents had a great impact on the fluorescence properties of the DPPPEA, as the combination of the electron-donating *para*-NPh_2 or *para*-9*H*-carbazolyl substituent with the electron-withdrawing Ph_2PO group provided an intrinsic D-A character in the excited state. Furthermore, attaching two *ortho*-methyl groups to the phenylene linker forced the neighboring carbazole ring to adopt an almost perpendicular orientation, preventing an effective π-conjugation via C–N linkages and dramatically changing the optical properties. The steady-state fluorescence spectra of the D-A type DPPPEAs measured in different solvents and at different temperatures revealed that the S_1 state is dominated by the LE character in weakly polar solvents or in rigid media, but by the CT character in polar and fluid solvents. The high fluorescence properties of the DPPPEAs were further demonstrated by the TTA phenomena using PtOEP as a photosensitizer; they emitted DF of 9.8–13.7 μs, corresponding to the 532-nm green laser irradiation. This study highlights the potential of the DPPPEAs as promising platforms for constructing tunable emitters and annihilators for use in a variety of optoelectronic devices. Further studies on the development of phosphorus-containing anthracene-based fluorophores are currently underway.

Experimental Section

General remarks: All melting points were recorded on a micro melting point apparatus and are uncorrected. NMR spectra were recorded on a 400 MHz (Agilent) spectrometer. The ^1H and ^{13}C chemical shifts are reported in ppm as relative values vs. tetramethylsilane (in $CDCl_3$) or a solvent residual signal (δ_H 7.16 ppm in C_6D_6), and the ^{31}P chemical shifts are reported in ppm vs. H_3PO_4. High-resolution mass (HRMS) spectra were measured on a Thermo Fisher Scientific EXACTIVE spectrometer (electron spray–quadrupole). UV/Vis absorption spectra were measured on a JASCO V-530 spectrometer or a Shimadzu UV-2600 spectrometer. The IR (Attenuated Total Reflection; ATR) spectra were obtained on a JASCO FT/IR4600 spectrometer. Electrochemical redox potentials were measured using a glassy carbon working electrode, a platinum wire counter electrode, and an Ag/Ag^+ [0.01 M $AgNO_3$, 0.1 M Bu_4NPF_6 (MeCN)] reference electrode. UV/Vis fluorescence spectra were measured on a JASCO FP-8300 spectrometer. Fluorescence quantum yields were measured on a Hamamatsu Photonics Quantaurus-QY spectrometer. Thin-layer chromatography was performed with Kieselgel 60 F254, and preparative column chromatography was performed using Silica Gel 60 spherical, neutrality. All reactions were performed under an argon or nitrogen atmosphere unless otherwise noted. For the experimental details and characterization data of new compounds are reported in the Supporting Information.

X-ray crystallographic analysis: Single crystals were grown from toluene–hexane (for **3a**, **3c**), CH_2Cl_2–hexane (for **3e**), toluene–MeOH (for **9**), or CH_2Cl_2–hexane–MeOH (for **10**) at room temperature. Deposition Numbers 2163729 (for **3a**), 2163730 (for **3c**), 2163731 (for **3e**), 2163732 (for **9**), 2163733 (for **10**) contain the supplementary crystallographic data for this paper. These data are provided free of charge by the joint Cambridge Crystallographic Data Centre and Fachinformationszentrum Karlsruhe Access Structures service. Selected structure parameters are as follows. **3a** (ccdc-2163729): $C_{34}H_{23}OP$, MW = 478.49, 0.10 × 0.10 × 0.10 mm, triclinic, *P*–1, $a = 8.5627(3)$ Å, $b = 9.7865(4)$ Å, $c = 16.1134(5)$ Å, $\alpha = 77.9270(10)°$, $\beta = 87.6340(10)°$, $\gamma = 67.7390(10)°$, $V = 1220.93(8)$ Å^3, $Z = 2$, $\rho_{calcd} = 1.302$ g cm^{-3}, $\mu = 1.39$ cm^{-1}, collected 107388, independent 5566, parameters 326, $R_w = 0.1756$ (all data), $R_1 = 0.0581$ ($I > 2.0\sigma(I)$), GOF = 1.308. **3c** (ccdc-2163730): $C_{49.5}H_{36}NOP$, MW = 691.76, 0.010 × 0.010 × 0.010 mm, triclinic, *P*–1, $a = 9.6989(19)$ Å, $b = 13.244(2)$ Å, $c = 15.273(3)$ Å, $\alpha = 76.700(3)°$, $\beta = 78.837(3)°$, $\gamma = 70.058(3)°$, $V = 1780.6(6)$ Å^3, $Z = 2$, $\rho_{calcd} = 1.290$ g cm^{-3}, $\mu = 0.43$ cm^{-1}, collected 41381, independent 8118, parameters 493, $R_w = 0.1113$ (all data), $R_1 = 0.0419$ ($I > 2.0\sigma(I)$), GOF = 1.054. **3e** (ccdc-2163731): $C_{35}H_{22}NOP$, MW = 503.50, 0.20 × 0.10 × 0.05 mm, orthorhombic, *P*bca, $a = 20.1338(5)$ Å, $b = 7.5324(2)$ Å, $c = 33.3524(9)$ Å, $\alpha = \beta = \gamma = 90°$, $V = 5058.1(2)$ Å^3, $Z = 8$, $\rho_{calcd} = 1.322$ g cm^{-3}, $\mu = 1.39$ cm^{-1}, collected 90658, independent 5786, parameters 343, $R_w = 0.1784$ (all data), $R_1 = 0.0717$ ($I > 2.0\sigma(I)$), GOF = 1.230. **9** (ccdc-2163732): $C_{49}H_{38}NO_2P$, MW = 703.77, 0.10 × 0.10 × 0.10 mm, monoclinic, $P2_1/c$, $a = 26.1957(9)$ Å, $b = 8.1181(3)$ Å, $c = 17.7240(7)$ Å, $\alpha = 90°$, $\beta = 102.7740(10)°$, $\gamma = 90°$, $V = 3675.9(2)$ Å^3, $Z = 4$, $\rho_{calcd} = 1.272$ g cm^{-3}, $\mu = 1.18$ cm^{-1}, collected 90712, independent 8426, parameters 482, $R_w = 0.1566$ (all data), $R_1 = 0.0659$ ($I > 2.0\sigma(I)$), GOF = 1.250. **10** (ccdc-2163733): $C_{48.5}H_{35}NOP$, MW = 714.19, 0.10 × 0.10 × 0.10 mm, orthorhombic, P_{bca}, $a = 27.849(5)$ Å, $b = 8.9305(13)$ Å, $c = 30.321(5)$ Å, $\alpha = \beta = \gamma = 90°$, $V = 7541(2)$ Å^3, $Z = 8$, $\rho_{calcd} = 1.258$ g cm^{-3}, $\mu = 1.02$ cm^{-1}, collected 167654, independent 8630, parameters 489, $R_w = 0.1870$ (all data), $R_1 = 0.0592$ ($I > 2.0\sigma(I)$), GOF = 1.140.

Fluorescence lifetime and triplet-triplet annihilation measurements: A sample solution in a 5-mm quartz tube was deoxygenated by bubbling with Ar for at least 10 min and then sealed with a plastic cap. A nanosecond YAG laser with a pulse width of 2 ns, a repetition frequency of 100 Hz, and wavelength of 355 nm (FTSS 355–150-I, CryLas) or 532 nm (FDSS 532–150-I, CryLas) was used as the excitation light source. Emission from the sample was captured by an optical fiber then passed through appropriate notch filter (REF-355.0-25 mm-A; REF-532.0-25 mm-A, Melles Griot) and simultaneously fed into the detectors. PL spectra were obtained with a multichannel spectrometer (PMA C10027, Hamamatsu). Time profiles of the emissions were measured by bringing the luminescence passed through appropriate band-pass filters (MC 610; MX0650, Asahi Spectra) into a photomultiplier tube (PMT; R7400 U-01, Hamamatsu). The output signals of the photomultiplier were then monitored with a digital oscilloscope (DPO7104, Tektronix). For the triplet–triplet annihilation measurements, commercially available PtOEP was used as a triplet sensitizer. The sample solution was excited with the YAG laser ($\lambda_{ex} = 532$ nm).

DFT calculations: The geometries were optimized by density functional theory (DFT) for the S_0 and T_1 states, and by time-dependent (TD) DFT for the S_1 state. The basis set used for the

© 2022 Wiley-VCH GmbH

optimization was 6–31G(d,p).[30] The functional of DFT and TDDFT was the Becke, three-parameter, Lee–Yang–Parr (B3LYP) exchange-correlation functional.[31] The optimized geometries were confirmed to be minima by vibrational analysis. The Cartesian coordinates and computed total energies are summarized in Table S1. The excitation energies and oscillator strengths listed in Table S5 were computed with the time-dependent density functional theory (TD-DFT) method. The solvent effects were incorporated in both the DFT and TD-DFT calculations using the solvation model based on density (SMD).[32] All the calculations were carried out using the Gaussian 16 suite of programs.[33]

Acknowledgements

This work was partially supported by JSPS KAKENHI (Grant Numbers: 18H01961, 21H04576 to Y. M.; 18K05036, 21K04980 to H. N.) and the Research Program of "Five-star Alliance" in "NJRC Mater. & Dev." (20214029) and a research grant from The Foundation for Japanese Chemical Research (492(R)) to T. I. We would also like to express our gratitude to the SPring-8 synchrotron facility, where synchrotron-radiation experiments were performed at the BL02B1 beamlines with the approval of the Japan Synchrotron Radiation Research Institute (JASRI) under proposal numbers 2020A0557, 2020A0834, 2020A1056, 2020A1644, 2020A1656, and 2021A1592.

Conflict of Interest

The authors declare no conflict of interest.

Data Availability Statement

The data that support the findings of this study are available from the corresponding author upon reasonable request.

Keywords: phosphorus · anthracene · acetylene · dyes/pigments · fluorescence

[1] M. Montalti, A. Credi, L. Prodi, M. T. Gandolfi, in *Handbook of Photochemistry*, CRC Press, Florida, **2000**.
[2] The S_1 energies of BPEA in solution and in the solid state were reported to be 2.64 and 2.40 eV, respectively, whereas its T_1 energy was estimated to be 1.1–1.2 eV. See: a) A. Demeter, *J. Phys. Chem. A* **2014**, *118*, 9985–9993; b) Y. J. Bae, G. Kang, C. D. Malliakas, J. N. Nelson, J. Zhou, R. M. Young, Y. L. Wu, R. P. Van Duyne, G. C. Schatz, M. R. Wasielewski, *J. Am. Chem. Soc.* **2018**, *140*, 15140–15144.
[3] For example, see: a) R. Giménez, M. Piñol, J. L. Serrano, *Chem. Mater.* **2004**, *16*, 1377–1383; b) O. S. Kwon, H. S. Song, J. Conde, H. Kim, N. Artzi, J. H. Kim, *ACS Nano* **2016**, *10*, 1512–1521; c) F. Zhong, J. Zhao, *Dyes Pigm.* **2017**, *136*, 909–918; d) K. Mase, Y. Sasaki, Y. Sagara, N. Tamaoki, C. Weder, N. Yanai, N. Kimizuka, *Angew. Chem. Int. Ed.* **2018**, *57*, 2806–2810; *Angew. Chem.* **2018**, *130*, 2856–2860; e) M. Hussain, A. M. El-Zohry, H. B. Gobeze, J. Zhao, F. D'Souza, O. F. Mohammed, *J. Phys. Chem. A* **2018**, *122*, 6081–6088; f) S. J. Ha, J. H. Kang, D. H. Choi, S. K. Nam, E. Reichmanis, J. H. Moon, *ACS Photonics* **2018**, *5*, 3621–3627; g) S. Jin, K. Sugawa, N. Takeshima, H. Tahara, S. Igari, S. Yoshinari, Y. Kurihara, S. Watanabe, M. Enoki, K. Sato, W. Inoue, K. Tokuda, T. Akiyama, R. Katoh, K. Takase, H. Ozawa, T. Okazaki, T. Watanabe, J. Otsuki, *ACS Photonics* **2018**, *5*, 5025–5037; h) F. Lu, T. Nakanishi, *Adv. Opt. Mater.* **2019**, *7*, 1900176; i) P. Bharmoria, H. Bildirir, K. Moth-Poulsen, *Chem. Soc. Rev.* **2020**, *49*, 6529–6554, and references therein.
[4] For example, see: a) S. Samori, S. Tojo, M. Fujitsuka, H.-J. Liang, T.-I. Ho, J.-S. Yang, T. Majima, *J. Org. Chem.* **2006**, *71*, 8732–8739; b) C. Teng, X. Yang, C. Yang, S. Li, M. Cheng, A. Hagfeldt, L. Sun, *J. Phys. Chem. C* **2010**, *114*, 9101–9110; c) F. Zhong, J. Zhao, *Dyes Pigm.* **2017**, *136*, 909–918; d) J. Isokuortti, S. R. Allu, A. Efimov, E. Vuorimaa-Laukkanen, N. V. Tkachenko, S. A. Vinogradov, T. Laaksonen, N. A. Durandin, *J. Phys. Chem. Lett.* **2020**, *11*, 318–324; e) Y. Lei, K. Chen, G. Tang, J. Zhao, G. G. Gurzadyan, *J. Photochem. Photobiol. A* **2020**, *398*, 112573, and references therein.
[5] For example, see: a) T. Oyamada, H. Sasabe, C. Adachi, S. Murase, T. Tominaga, C. Maeda, *Appl. Phys. Lett.* **2005**, *86*, 033503; b) C. H. Chien, C. K. Chen, F. M. Hsu, C. F. Shu, P. T. Chou, C. H. Lai, *Adv. Funct. Mater.* **2009**, *19*, 560–566; c) S. O. Jeon, J. Y. Lee, *J. Mater. Chem.* **2012**, *22*, 4233–4243; d) C. Liu, Y. Li, Y. Li, C. Yang, H. Wu, J. Qin, Y. Cao, *Chem. Mater.* **2013**, *25*, 3320–3327; e) G. Mallesham, C. Swetha, S. Niveditha, M. E. Mohanty, N. J. Babu, A. Kumar, K. Bhanuprakash, V. J. Rao, *J. Mater. Chem. C* **2015**, *3*, 1208–1224; f) C. Li, C. Duan, C. Han, H. Xu, *Adv. Mater.* **2018**, *30*, 1804228; g) X. Song, H. Xu, *J. Inf. Disp.* **2020**, *21*, 149–172, and references therein.
[6] Z. Fei, N. Kocher, C. J. Mohrschladt, H. Ihmels, D. Stalke, *Angew. Chem. Int. Ed.* **2003**, *42*, 783–787; *Angew. Chem.* **2003**, *115*, 807–811.
[7] a) Z. Jiang, M. Xu, F. Li, Y. Yu, *J. Am. Chem. Soc.* **2013**, *135*, 16446–16453; b) M. Xu, C. Han, Y. Yang, Z. Shen, W. Feng, F. Li, *J. Mater. Chem. C* **2016**, *4*, 9986–9992.
[8] Y. Zhao, L. Duan, X. Zhang, D. Zhang, J. Qiao, G. Dong, L. Wang, Y. Qiu, *RSC Adv.* **2013**, *3*, 21453–21460.
[9] R. Tao, J. Zhao, F. Zhong, C. Zhang, W. Yang, K. Xu, *Chem. Commun.* **2015**, *51*, 12403–12406.
[10] H.-B. Xu, J. Wang, X.-L. Chen, P. Xu, K.-T. Xiong, D.-B. Guan, J.-G. Deng, Z.-H. Deng, M. Kurmoo, M.-H. Zeng, *Dalton Trans.* **2018**, *47*, 6908–6916.
[11] In this paper, we use DPPPEA in comparison with BPEA and BDPPA. In light of the IUPAC nomenclature, the name of this compound is diphenyl(10-(phenylethynyl)anthracen-9-yl)phosphine oxide.
[12] G. Schwab, D. Stern, D. Leusser, D. Stalke, *Z. Naturforsch. B* **2007**, *62*, 711–716.
[13] The structures of 9-diisopropylphosphanylanthracene derivatives were studied by NMR spectroscopy. See: G. Schwab, D. Stern, D. Stalke, *J. Org. Chem.* **2008**, *73*, 5242–5247.
[14] T. A. Albright, W. J. Freeman, E. E. Schweizer, *J. Org. Chem.* **1975**, *40*, 3437–3441.
[15] C. Wang, Y. Liu, Z. Ji, E. Wang, R. Li, H. Jiang, Q. Tang, H. Li, W. Hu, *Chem. Mater.* **2009**, *21*, 2840–2845.
[16] Stalke et al. have studied in detail the relationship between the solid-state structures and the fluorescence properties of related (diphenylthiophosphoryl)anthracene derivatives. See: a) T. Schillmöller, P. N. Ruth, R. Herbst-Irmer, D. Stalke, *Chem. Commun.* **2020**, *56*, 7479–7482; b) T. Schillmöller, P. N. Ruth, R. Herbst-Irmer, D. Stalke, *Chem. Eur. J.* **2020**, *26*, 17390–17398; c) T. Schillmöller, R. Herbst-Irmer, D. Stalke, *Adv. Opt. Mater.* **2021**, *9*, 2001814.
[17] The hydrogen-bonding interaction between the P=O group of **3a** and H–O group of the solvent appeared as a slight downfield shift of its ^{31}P signal ($\delta_P = 31.0$ in CD_3OD; 31.3 in $CDCl_3$).
[18] F. Zhong, J. Zhao, *Dyes Pigm.* **2017**, *136*, 909–918.
[19] The redox potential of +1.30 V vs. SCE was converted to that vs. Fc/Fc^+. See: L. Sicard, C. Quinton, F. Lucas, O. Jeannin, J. Rault-Berthelot, C. Poriel, *J. Phys. Chem. C* **2019**, *123*, 19094–19104.
[20] J. G. Kirkwood, *J. Chem. Phys.* **1939**, *7*, 911–919.
[21] G. Åkerlöf, *J. Am. Chem. Soc.* **1932**, *54*, 4125–4139.
[22] F. Buckley, A. A. Maryott, in *National Bureau Standards Circular 589*, United States Department of Commerce, N. B. o. S., Ed.; Washington, U. S., **1958**.
[23] D. R. Lide, in *CRC Handbook of Chemistry and Physics*, 86th Ed., Taylor and Francis, Florida, **2005**, 6–132-6–152.
[24] M. Kytka, L. Gisslen, A. Gerlach, U. Heinemeyer, J. Kováč, R. Scholz, F. Schreiber, *J. Chem. Phys.* **2009**, *130*, 214507.
[25] I. R. Gould, R. H. Young, R. E. Moody, S. Farid, *J. Phys. Chem.* **1991**, *95*, 2068–2080.
[26] We adopted a 4.8 Å radius of the solvent cavity for a solute molecule, which was estimated from the molecular structure clarified by the X-ray diffraction analysis of **3c**.
[27] a) W. Li, Y. Pan, L. Yao, H. Liu, S. Zhang, C. Wang, F. Shen, P. Lu, B. Yang, Y. Ma, *Adv. Opt. Mater.* **2014**, *2*, 892–901; b) S. Sasaki, G. P. C. Drummen,

© 2022 Wiley-VCH GmbH

G. Konishi, *J. Mater. Chem. C* **2016**, *4*, 2731–2743; c) Y. Gao, S. Zhang, Y. Pan, L. Yao, H. Liu, Y. Guo, Q. Gu, B. Yang, Y. Ma, *Phys. Chem. Chem. Phys.* **2016**, *18*, 24176–24184; d) T. Liu, X. Chen, J. Zhao, W. Wei, Z. Mao, W. Wu, S. Jiao, Y. Liu, Z. Yang, Z. Chi, *Chem. Sci.* **2021**, *12*, 5171–5176, and references therein.

[28] The T_1 energy of PtOEP was reported to be 1.9 eV. See: M. A. Baldo, S. R. Forrest, *Phys. Rev. B* **2000**, *62*, 10958–10966.

[29] K. Yokoyama, Y. Wakikawa, T. Miura, J.-i. Fujimori, F. Ito, T. Ikoma, *J. Phys. Chem. B* **2015**, *119*, 15901–15908.

[30] a) R. Ditchfield, W. J. Hehre, J. A. Pople, *J. Chem. Phys.* **1971**, *54*, 724–728; b) W. J. Hehre, R. Ditchfield, J. A. Pople, *J. Chem. Phys.* **1972**, *56*, 2257–2261; c) P. C. Hariharan, J. A. Pople, *Theor. Chim. Acta* **1973**, *28*, 213–222; d) M. S. Gordon, J. S. Binkley, J. A. Pople, W. J. Pietro, W. J. Hehre, *J. Am. Chem. Soc.* **1982**, *104*, 2797–2803; e) M. M. Francl, W. J. Pietro, W. J. Hehre, J. S. Binkley, M. S. Gordon, D. J. DeFrees, J. A. Pople, *J. Chem. Phys.* **1982**, *77*, 3654–3665.

[31] a) A. D. Becke, *J. Chem. Phys.* **1993**, *98*, 5648–5652; b) C. Lee, W. Yang, R. G. Parr, *Phys. Rev. B* **1988**, *37*, 785–789.

[32] A. V. Marenich, C. J. Cramer, D. G. Truhlar, *J. Phys. Chem. B* **2009**, *113*, 6378–6396.

[33] *Gaussian 16, Revision C.01*; M. J. Frisch, G. W. Trucks, H. B. Schlegel, G. E. Scuseria, M. A. Robb, J. R. Cheeseman, G. Scalmani, V. Barone, G. A. Petersson, H. Nakatsuji, X. Li, M. Caricato, A. V. Marenich, J. Bloino, B. G. Janesko, R. Gomperts, B. Mennucci, H. P. Hratchian, J. V. Ortiz, A. F. Izmaylov, J. L. Sonnenberg, D. Williams-Young, F. Ding, F. Lipparini, F. Egidi, J. Goings, B. Peng, A. Petrone, T. Henderson, D. Ranasinghe, V. G. Zakrzewski, J. Gao, N. Rega, G. Zheng, W. Liang, M. Hada, M. Ehara, K. Toyota, R. Fukuda, J. Hasegawa, M. Ishida, T. Nakajima, Y. Honda, O. Kitao, H. Nakai, T. Vreven, K. Throssell, J. A. Montgomery, Jr., J. E. Peralta, F. Ogliaro, M. J. Bearpark, J. J. Heyd, E. N. Brothers, K. N. Kudin, V. N. Staroverov, T. A. Keith, R. Kobayashi, J. Normand, K. Raghavachari, A. P. Rendell, J. C. Burant, S. S. Iyengar, J. Tomasi, M. Cossi, J. M. Millam, M. Klene, C. Adamo, R. Cammi, J. W. Ochterski, R. L. Martin, K. Morokuma, O. Farkas, J. B. Foresman, D. J. Fox, Gaussian, Inc., Wallingford CT, 2019.

Manuscript received: April 7, 2022
Revised manuscript received: May 11, 2022
Accepted manuscript online: May 18, 2022
Version of record online: June 13, 2022

© 2022 Wiley-VCH GmbH